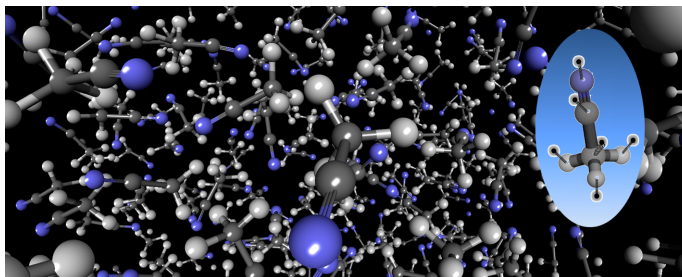


1 Graphical Abstract

2 **A General Purpose Acetonitrile Interaction Potential to Describe its Liquid, Solid and Gas**  
3 **Phases**

4 Jorge Hernández-Cobos, José M. Martínez, Rafael R. Pappalardo, Iván Ortega-Blake, Enrique Sánchez Marcos



5

# 1 Highlights

## 2 **A General Purpose Acetonitrile Interaction Potential to Describe its Liquid, Solid and Gas** 3 **Phases**

4 Jorge Hernández-Cobos, José M. Martínez, Rafael R. Pappalardo, Iván Ortega-Blake, Enrique Sánchez Marcos

- 5 • Acetonitrile flexible and polarizable force field based on quantum mechanical computations
- 6 • MD simulations of gas phase clusters, liquid, and  $\alpha$  and  $\beta$  crystal structures
- 7 • Satisfactory comparison of simulated and experimental physicochemical properties

# A General Purpose Acetonitrile Interaction Potential to Describe its Liquid, Solid and Gas Phases<sup>\*</sup>

Jorge Hernández-Cobos<sup>a</sup>, José M. Martínez<sup>b</sup>, Rafael R. Pappalardo<sup>b</sup>, Iván Ortega-Blake<sup>a</sup> and Enrique Sánchez Marcos<sup>b</sup>

<sup>a</sup>Instituto de Ciencias Físicas, UNAM, Apartado Postal 48-3, 62251-Cuernavaca, México

<sup>b</sup>Department of Physical Chemistry, University of Sevilla, 41012-Sevilla, Spain

## ARTICLE INFO

### Keywords:

ab initio force field  
polarizable and flexible acetonitrile model  
MD simulations  
x-ray and neutron diffractograms  
physicochemical properties  
acetonitrile crystals

## ABSTRACT

A flexible and polarizable force field to describe acetonitrile in its three states of matter has been developed on the basis of an ab initio potential energy surface at the MP2 level. The acetonitrile molecule is represented by a sophisticated twelve-site model: the six nuclei plus six mobile charges. Three thousands structures have been employed for the fitting including monomers, dimers and trimers. Gas phase behavior has been tested by analyzing aggregates from dimers to 27-mer which give accurate reproducibility of the experimental and quantum-mechanical results. Classical MD simulations have been performed for the liquid and its crystalline  $\alpha$ - and  $\beta$ -forms. An analysis of liquid in a wide range of structural, dynamic, energetics and spectroscopic properties has been performed, as well as neutron diffraction data. Comparison with experimental information is satisfactory. Due to the first principles nature and the polarizable character of this force field properties of the three states of matter are properly reproduced.


## 1. Introduction

Acetonitrile (ACN) is one of the most used polar aprotic solvents, more precisely a dipolar non-hydrogen bonded solvent.[1] ACN combines a high relative permittivity, low viscosity, differential solvation behavior against cations and anions, and an amphiphilic character provided by the presence of the methyl group and a strong dipolar charge distribution of the molecule. The concurrence of all these features makes this solvent extremely versatile in manifold technological areas such as chemical and pharmaceutical industries,[2, 3], electrochemistry and organic and inorganic synthesis.[1, 4] Even more, ACN plays a double role as solvent and reactant in solution as well as in the acetonitration of gaseous aggregates.[5, 6]

A thorough understanding of the physicochemical properties of liquid ACN and its solutions needs their structural characterization, not only to explain the observed behavior but also to envisage the study of more complex chemical systems, and the extension to new applications in gas phase[6] and solid state. An excellent review of Pothoczki et al.[7], appeared in 2015, compiles the experimental and theoretical efforts to deal with liquid ACN. The set of experimental x-ray and neutron diffraction studies[8–12] has been complemented in Table 1 with several theoretical methods to get insight into the structural interpretation at the atomistic level.[13–25]

The number of particles needed to describe the condensed medium, the performance of the available DFT methods, as well as the long simulation times required to estimate certain properties limit the use of ab initio MD simulations.[26, 27] Then, most of the statistical simulations are classical and the treatment of the condensed phase relies on the force fields describing the interactions among particles. Different strategies have been adopted to provide good-behaving interaction potentials, considering on one hand, the flexibility or rigidity of the ACN molecule and on the other the polarizable character of the molecule. Likewise, the data used to build the force field could be from experimental or first principles origin. In the first case, the potential parameters are fitted to reproduce as well as possible some selected experimental properties. In the second case, the fitting is based on the reproduction of quantum mechanical results of the ACN monomer and, in general, the dimer interaction in a large number of attractive and repulsive arrangements. Table 1 collects the force fields available in the literature with indication of their main features and computed properties. Most of them are able to supply good descriptions of a set of ACN liquid

\*Corresponding author

 sanchez@us.es (E. Sánchez Marcos)

ORCID(s): 0000-0002-8367-9105 (E. Sánchez Marcos)

properties whose range of applicability is determined by both, the type of model defined and the set of data used for the fitting. In a recent and clarifying study, Kowsari et al.[13] have performed a systematic evaluation of the ACN force fields which use a six-site model and molecular flexibility.[14, 15, 17, 20] They compared on the same foot the performance of these potentials on a set of thermodynamic and transport properties of liquid ACN. These authors point out the difficulty of satisfying simultaneously very accurate description of thermodynamic and transport properties. Thus, the Grabuleda et al.'s potential[20] and that of Nikitin et al.[17] supply good description of the density of the vaporization enthalpy, but they provide less accurate values of the self-diffusion coefficient. Contrarily, Orhan[15] builds a force field where the transport properties, the dielectric relaxation and vibrational spectra of bulk ACN were well reproduced along a wide temperature range. However, Kowsari et al.[13] show that the density and the vaporization enthalpy are underestimated by Orhan's potential. Koverga et al.[14] adopt an intermediate strategy to develop their force field since they fit parameters to reproduce simultaneously thermodynamic and transport properties. They get a good potential which is able to predict properly density, vaporization enthalpy and diffusion coefficient compared to the rest of available simulated data. Nevertheless, overall the dynamic properties show a lower accuracy relative to thermodynamic estimates.[14] On the basis of this analysis, Kowsari et al.[13] performed a refinement process tuning some of the Lennard-Jones parameters of the potentials to fit the available experimental data. The refined potential is able to reproduce both thermodynamic and dynamic properties of liquid ACN pretty well.

It must be noted, that there is no purely first-principles interaction potential including polarizability and flexibility on a fully atomic representation of the ACN molecule. In this work we do build such a force field type, in addition of including many-body corrections. To this end we have developed a twelve-site model. The aim is to check the performance of this purely first-principles force field, not only in liquid state but also in gas phase clusters and solid state crystals. Since no experimental information is used for the force field building, the inclusion of enough many-body contributions should allow a proper description of all the aggregation states involving ACN molecules. The gas phase was studied on ACN clusters of different sizes and the solid state in two well-characterized crystal forms,  $\alpha$  and  $\beta$ . [28–30]

Table 1: Computer simulation studies of ACN based on classical interaction potentials.

Author[Ref.]	Potential Nature		Potential Fitted to <sup>(a)</sup>	Properties <sup>(a)</sup>
	Geometry	Charge Distrib.		
Kowsari [13]	Flexible	Non-Polarizable	Exp. data of $\rho$ , $V_m$ , $\Delta H_{\text{vap}}$ , C.E.D. and D	$\rho$ , $V_m$ , $\Delta H_{\text{vap}}$ , C.E.D., D, RDF, CDF
Koverga [14]	Flexible	Non-Polarizable	CPMD, QM, Exp. data	RDF, CDF, Nearest neighbors analysis, Dielectric properties, H-bond interactions
Orhan [15]	Flexible	Non-Polarizable	Exp. data	RDF, Liquid vibration spectra at different T, $\eta_s$ , $D$ , $\tau_1$ , $\tau_2$ , Dielectric properties
Alberti [16]	Rigid	Non-polarizable	Atom polarizabilities	$E_{\text{config}}$ as a function of T ( $\text{CH}_3\text{CN}$ ) <sub>n</sub> , n=2-4 $D$ and $\rho$ as a function of T RDF, Ion-ACN solutions
Nikitin [17]	Flexible	Non Polarizable	Exp. data of $\rho$ , $\Delta H_{\text{vap}}$	RDF, $\rho$ of ACN-water solutions, Dielectric properties, $D$
Gee [18]	Flexible	Non-polarizable	Exp. data	$\Delta H_{\text{vap}}$ , $\rho$ , $C_p$ , $\epsilon$ , $D$ , $\eta$ , $\tau_1$ , $\tau_2$ , RDF

Author[Ref.]/Pot. Name	Potential Nature		Fitted to	Properties
	Geometry	Charge Distrib.		
Sum [31]	Rigid	Non-Polarizable & Polarizable	Scaled <i>ab initio</i> 2nd. Virial Co-efficient	$\Delta H_{\text{vap}}$ , Gas-Liquid Coexistence: $T_c, \rho_c$ RDF
Guardia [19]	Rigid	Non-Polarizable	<i>ab initio</i> calculations of dimer	$\rho, V_m, \Delta H_{\text{vap}}, \kappa, C_p$ RDF, X-ray structure factor, $D, \tau_1, \tau_2$ Dielectric properties ( $G_k, y, \epsilon_0, \epsilon_0 - \epsilon_\infty, g_k, \tau_\varphi, \tau_D, \tau_D/\tau$ )
Grabuleda [20]	Flexible	Non-polarizable	Exp. data	$\rho, \kappa, \Delta H_{\text{vap}}, \mu, \text{RDF}$
Cabaleiro-Lago [21]	Rigid	Polarizable	<i>ab initio</i> IMPT data HF/MP2/6-31G**	Dimer energy, geometry and frequencies Trimer and tetramer energy and geometry $U, \text{RDF}$ , Dipole moment distribution, Dipole-Dipole angle distribution
Siebers [22]	Flexible	Non-Polarizable	Exp. data	Minimum energy structures of ACN clusters from $n = 2$ to $n = 13$ Frequency shifts of the CC stretch and the $\text{CH}_3$ wag modes
Jorgensen [23]	Rigid	Non-Polarizable	Exp. Data	$\rho, V_M, U, \Delta H_{\text{vap}}, \kappa, C_p, \text{RDF}$ , Energy distribution functions, RDF, Dipole correlation
Edwards [24]	Rigid	Non-Polarizable	Six site model	Dielectric Properties Center of mass $G(r)$ Orientational correlation functions Dipole correlation functions
Böhm [25]	Rigid	Non-Polarizable	Exp. data	$U, \kappa, C_p, \text{RDF}, D, \tau_2$ Neutron and X-Ray Scattering

- <sup>1</sup> <sup>(a)</sup>  $\rho$  = density;  $V_m$  = molar volume; C.E.D.= Cohesive energy density;  
<sup>2</sup> CDF=Combined distribution function;  $\eta$ = shear viscosity;  $D$ = self-diffusion coefficient;  
<sup>3</sup>  $\tau_i = i^{\text{th}}$ -order reorientational time;  $C_p$ =heat capacity at constant pressure;  $\kappa$ = isothermal compressibility.

## 4 2. Methods

### 5 2.1. Potential Development

<sup>6</sup> In this work we build a force field for acetonitrile whose functional form is based on the Mobile Charge Densities  
<sup>7</sup> in Harmonic Oscillators (MCDHO) model [32, 33]. This allows for the inclusion of intramolecular flexibility, non-  
<sup>8</sup> additivity and polarizability. The molecular polarizability is accounted by a set of negative mobile charge densities  
<sup>9</sup> with radial exponential decay associated to each positively charged nuclei. The interaction between both charges is

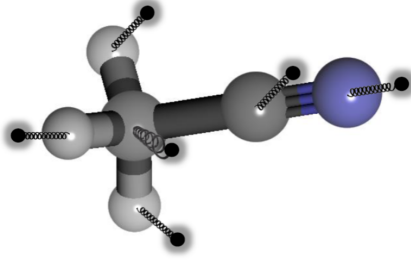


**Figure 1:** Molecular model used to define the acetonitrile molecule.

described by means of a harmonic oscillator. The remaining charge-charge interactions in the system consider the charges as points. A mobile charge has been associated to each ACN nucleus, thus we build a twelve-site model formed by the sum of six nuclei plus six mobile charges. Figure 1 displays a scheme of the ACN molecular model.

The specific expression for the water - water interaction in the MCDHO model was given in eqs. (4-6) of Ref.[32]. The molecular complexity of acetonitrile requires a more general formulation that we detail at this point. A previous force field, developed for liquid methanol [34], uses a model definition similar to that here presented. However, in that case hard core cutoff radii for the interactions were included in the potential limiting its use to Monte Carlo simulations. For the ACN we developed a potential with a good behavior of the energy gradients, allowing for its use in Molecular Dynamics simulations.

The total energy is the sum of an intramolecular and an intermolecular energy. In the following equations  $r_{ij} = |\mathbf{r}_i - \mathbf{r}_j|$  is the distance between the corresponding centers, either fixed positive nuclei  $Z$  or mobile negative charges  $q$ , where  $i$  and  $j$  subscripts correspond to sites  $i$  and  $j$ .

The analytical expression to compute the intramolecular energy is the sum of the following contributions:

$$U_{\text{intra}} = \sum_{i \in S} \sum_{j > i} [U(Z_i, Z_j) + U(q_i, q_j)] + \sum_{i \in S} \sum_{j \neq i} U(q_i, Z_j) + \sum_{i \in S} \frac{1}{2} k_i r_{ii}^2 \quad (1)$$

$$+ \sum_{\text{bonds}} U_b(i, j) + \sum_{\text{angles}} U_\theta(i, j, k)$$

where the first two terms correspond to the electrostatic interactions among nuclei and mobile charges, the third term corresponds to the harmonic energy of the mobile charge at a distance  $r_{ii}$  from its nucleus, and the other two terms correspond to the bond energy and the bond angle energy. The summation  $i \in S$  runs over atomic centers of the molecule. These terms do have the following functional forms:

1. The electrostatic interaction between nuclei:

$$U(Z_i, Z_j) = \frac{Z_i Z_j}{r_{ij}} \quad (2)$$

2. The interaction between mobile charges with decay lengths  $\lambda_i$  and  $\lambda_j$  attached to bonded atoms. In this case a two-center integral should be used; however, an approximate expression that gives good accuracy at all relevant distances was found[32, 33]:

$$U(q_i, q_j) = \frac{q_i q_j}{r_{ij}} \left[ 1 - \left( \frac{\lambda_i \lambda_j + (\lambda_i + \lambda_j)^2}{(\lambda_i + \lambda_j)^3} r_{ij} + 1 \right) \exp \left( -2 \frac{\lambda_i \lambda_j + (\lambda_i + \lambda_j)^2}{(\lambda_i + \lambda_j)^3} r_{ij} \right) \right] \quad (3)$$

mobile charge densities are considered as point charges when interacting with mobile charge densities of non-bonded atoms

$$U(q_i, q_j) = \frac{q_i q_j}{r_{ij}} \quad (4)$$

3. The electrostatic interaction between mobile charge densities  $q_i$  and an atomic center charge  $Z_j$  to which its own atom is bonded, where  $\lambda_i$  is the intramolecular decay length of the charge density:

$$U(q_i, Z_j) = \frac{q_i Z_j}{r_{ij}} \left[ 1 - \left( \frac{r_{ij}}{\lambda_i} + 1 \right) \exp \left( -\frac{2r_{ij}}{\lambda_i} \right) \right] \quad (5)$$

The mobile charge densities are considered as point charges when interacting with a non-bonded atomic center. In these cases the electrostatic interaction is given by:

$$U(q_i, Z_j) = \frac{q_i Z_j}{r_{ij}} \quad (6)$$

4. A Morse potential between each pair of bonded atoms, with depth  $D_{ij}$ , inverse decay length  $\gamma_{ij}$  and equilibrium parameter  $r_{ij}^{eq}$ :

$$U_b(i, j) = D_{ij} \left\{ \exp \left[ -2\gamma_{ij} (r_{ij} - r_{ij}^{eq}) \right] - \exp \left[ -\gamma_{ij} (r_{ij} - r_{ij}^{eq}) \right] \right\} \quad (7)$$

5. A quadratic term for each bond angle  $\theta_{ijk}$ , with parameter  $k_\theta$  and the equilibrium value  $\theta_{ijk}^0$ :

$$U_\theta(i, j, k) = \frac{k_\theta}{2} (\theta_{ijk} - \theta_{ijk}^0)^2 \quad (8)$$

The intermolecular energy is composed of the following terms:

$$U_{\text{inter}} = \sum_{S=1}^N \left( \sum_{T=1}^{S-1} \left\{ \sum_{i \in S} \sum_{j \in T} \left[ U_{\text{inter}}(Z_i, Z_j) + U_{\text{inter}}(q_i, Z_j) + U_{\text{inter}}(q_j, Z_i) + U_{\text{inter}}(q_i, q_j) \right] \right\} \right) \quad (9)$$

where summations  $i \in S$  and  $j \in T$  refer to entire molecules and the expression of each term is:

1. The electrostatic interactions between atomic centers plus exponential terms with parameters  $A_{ij}$ ,  $B_{ij}$ ,  $a_{ij}$  and  $b_{ij}$ :

$$U_{\text{inter}}(Z_i, Z_j) = A_{ij} \exp(-a_{ij} r_{ij}) + B_{ij} \exp(-b_{ij} r_{ij}) + \frac{Z_i Z_j}{r_{ij}} \quad (10)$$

2. The electrostatic interaction between mobile charges  $q_i$  considered as point charges and charges  $Z_j$ :

$$U_{\text{inter}}(q_i, Z_j) = \frac{q_i Z_j}{r_{ij}} \quad (11)$$

3. The electrostatic interaction between mobile charges,

$$U_{\text{inter}}(q_i, q_j) = \frac{q_i q_j}{r_{ij}}, \quad (12)$$

Therefore, the energy of a cluster with  $N$  molecules is given by,

$$U_{\text{total}} = U_{\text{inter}} + \sum_{S=1}^N U_{\text{intra}}(S), \quad (13)$$

The interaction energy,  $U_{\text{int}}$ , for a cluster of  $N$  molecules requires the subtraction of the intramolecular energies of the isolated molecules,  $U_{\text{intra}}^0$ , that corresponds to the  $U_{\text{intra}}$  value in eq. (1) for an ACN molecule at its optimized geometry.

$$U_{\text{int}} = U_{\text{total}} - \sum_{S=1}^N U_{\text{intra}}^0(S) = U_{\text{total}} - NU_{\text{intra}}^0, \quad (14)$$

thus, taking into consideration the energetic cost of polarizing and deforming each molecule in the cluster or condensed phases.

Due to the large number of parameters to be fitted in this potential and the different nature of the interactions, the set of ACN structures chosen to be fitted from the *ab initio* potential energy surfaces were chosen in an iterative manner. Likewise, the different set of parameters were included sequentially in the fitting process as well. That is, initial structures were taken from a regular scan of the ACN molecule hyper-surface with respect to their different internal degrees of freedom. An initial potential parameterization was fitted for the intramolecular part of the potential,  $U_{\text{intra}}$ . This potential was used to generate a set of new structures derived from numerical simulations at standard temperature. These new structures were then computed at the *ab initio* level and added to the set of structures employed to fit the potential. This procedure is repeated until convergence is achieved. A scheme of this iterative process was sketched in a previous work where a Cf(III)-H<sub>2</sub>O potential was built.[35]. Once a fitting of the intramolecular potential was achieved, ACN dimers were included in the energy surface, scanning intermolecular distances and orientations. Then, the same iterative procedure was used for the intermolecular part adding dimer interaction energies and non-additivities computed from trimers. Hence, the final surfaces to be fitted consisted of: (a) the three components of the dipole moment of the optimal monomer and the dipole moment modulus of all distorted ACN monomers. (b) 1117 monomer structures where the deformation energy, relative to the optimal monomer, was considered for fitting, (c) 1980 dimer structures where the interaction energy was fitted, (d) 61 trimer structures where the three-body non additive contributions were fitted.

The quality of the fitting is shown in Figure 2 where the total interaction energy,  $U_{\text{int}}$  in eq. (14), computed by the force field for the employed set of 3158 structures is compared with the corresponding *ab initio* values. The standard deviation of this comparison is 0.29 kcal/mol. Due to the fitting procedure four different standard deviation can be evaluated: that of the monomer deformation energies, 0.25 kcal/mol, that of the dimer interaction energies, 0.28 kcal/mol, that of the many-body interactions associated to the trimers, 0.04 kcal/mol, and that of the dipole moment evaluation of monomers, 0.11 D. The potential parameters are presented in Table S1 of Supplementary Material (SM).

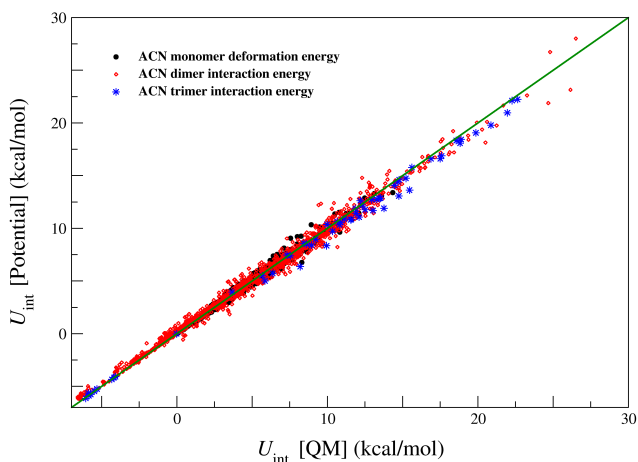
Molecular orbital calculations were done with the Gaussian09 program [36]. The computational level chosen was MP2/6-311++G(3df,3pd). Interaction energies were corrected of basis set superposition errors by using the counterpoise method.

Table 2 collects the geometrical parameters corresponding to an ACN molecule and its most stable dimer obtained by the quantum-mechanical calculation, the developed potential, results obtained by other authors and experimental data. Both the degree of reproducibility of the basic molecular properties and intermolecular interactions are satisfactory. Table S2 of SM collects the comparison of the frequencies of the main vibrational normal modes of the ACN molecule obtained by the force field with those derived from the QM level used for the fitting and with the experimental ones. More demanding tests to assess the good performance of the developed potential, when a large number of ACN molecules are interacting, are presented in the Results Section.

## 2.2. Molecular Dynamics Simulation Details

Molecular dynamics (MD) simulations were run using a modified version of *DL\_POLY\_CLASSIC* [45] which allows the use of the MCDHO force field. An integration time step of 0.05 fs was used to account properly for the high frequencies associated to the dynamics of the mobile charges. The Ewald Summation was used to calculate the





**Figure 2:** Comparison between the interaction energies,  $U_{\text{int}}$  predicted by the force field developed and the *ab initio* ones for the set of structures employed for the fit.

**Table 2**

Basic properties of ACN molecule and its dimer.

Property	QM	Potential	Literature <sup>a</sup>	Exptal. <sup>b</sup>
monomer				
$R_{\text{C-C}}$ (Å)	1.458	1.457	1.441-1.464	1.458
$R_{\text{C-N}}$ (Å)	1.168	1.170	1.159-1.181	1.157
$R_{\text{C-H}}$ (Å)	1.087	1.087	1.093-1.109	1.104
$\Theta_{\text{CCH}}$ (°)	109.0	109.0	109.0-110.5	109.5
$\mu$ (D)	4.3	4.0	3.98-4.12	3.9
dimer				
$R$ (C <sub>N</sub> ...C <sub>N</sub> ) (Å)	3.291	3.369	3.096-3.502	
$R$ (N...H) (Å)	2.468	2.563	2.450-2.601	
$\Theta$ (N-C...C <sub>N</sub> ) (Å)	134.9	134.3	132.9-139.3	
$U_{\text{int}}$ (kcal/mol)	-6.21	-6.22	(-3.08)-(-9.85)	-5.0

<sup>a</sup>Refs. [16, 37-39] <sup>b</sup>Refs. [40-44]

1 electrostatic interactions. The van der Waals interactions were truncated at a cutoff radius of 14 Å. The Nosé-Hoover  
2 thermostat to attain the average target temperature was applied with a characteristic time of 0.5 ps. The Nosé-Hoover  
3 barostat with a characteristic time of 1.0 ps was applied to keep the average pressure at 1 atm. 500 ACN molecules were  
4 explicitly considered in the simulation box for the liquid ACN simulation at 298 K. The system was minimized and an  
5 NPT run of 0.5 ns to equilibrate the simulation box was performed. 1 ns production simulation was used for further  
6 analysis and extraction of physicochemical properties. Additionally, a similar NVT MD simulation at the experimental  
7 density at 298 K was also performed to compare with the NPT results. The translational self-diffusion coefficient,  $D^0$ ,  
8 for ACN in the MD simulation was computed using the Einstein formula[46] and corrected for finite box-size effects  
9 with the Yeh and Hummer' formula [47]:

$$D_{\text{ACN}}^{\text{corr}} = D_{\text{ACN}}^0 + \frac{k_B T \xi}{6\pi\eta L} \quad (15)$$

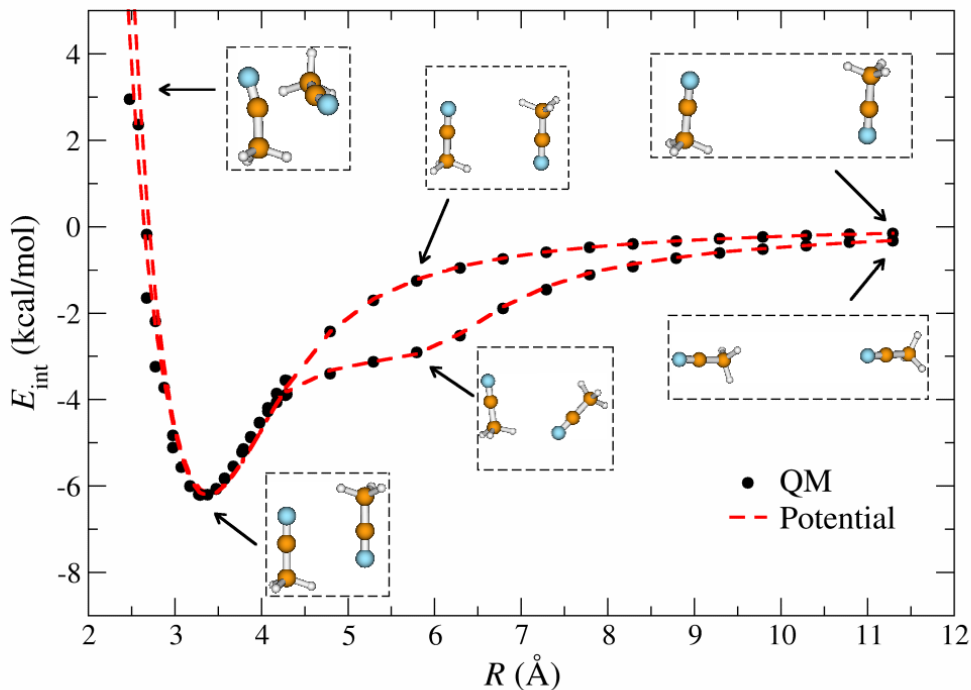


**Figure 3:** Comparison of QM (black dots) and potential-derived (red line) dissociation curves (kcal/mol) of the ACN minimal energy dimer. At short distances the two curves collapse to the head to tail antiparallel arrangement.

1 where  $\eta$  is the ACN viscosity,  $L$  the box length, and  $\xi$  the self-term for a cubic box (2.8373 at room temperature).  
 2 The correction term depends on the viscosity. Usually the experimental value for the liquid at the target temperature is  
 3 used. However, in this case for the sake of consistency and as a double check of our potential, we have computed the  
 4 shear-viscosity using the Green-Kubo approach. The shear-viscosity is computed by integrating over time the pressure  
 5 tensor autocorrelation function as given by the following equation

$$\eta = \frac{V}{k_B T} \int_0^\infty \langle P_{\alpha\beta}(t) P_{\alpha\beta}(0) \rangle dt \quad (16)$$

6 where  $P_{\alpha\beta}$  is the  $\alpha\beta$  element of the pressure tensor,  $V$  is the volume system and  $T$  the working temperature. The angle  
 7 brackets inside the integral denote that it is computed the average of the ensemble.[48] We have followed the time  
 8 decomposition method proposed by Maginn and col.[49] to evaluate the integral.

9 Uncertainties of all simulated properties are given as standard error.

### 10 3. Results and Discussion

#### 11 3.1. Potential assessment: clusters in gas phase

12 The first test of the new potential was the computation of the interaction energy associated to the dissociation curves  
 13 between two molecules arranged according to the two lowest energy orientations, i.e. the linear and antiparallel head  
 14 to tail orientations. Figure 3 displays the curves predicted by the potential (red lines) and those obtained at the QM  
 15 level (black dots). The  $R$  value used in the abscissas axis corresponds to the  $C_N-C_N$  distance, which is roughly the  
 16 molecular center of mass separation. Each curve has been computed fixing the  $R(C_N-C_N)$  and allowing the relaxation

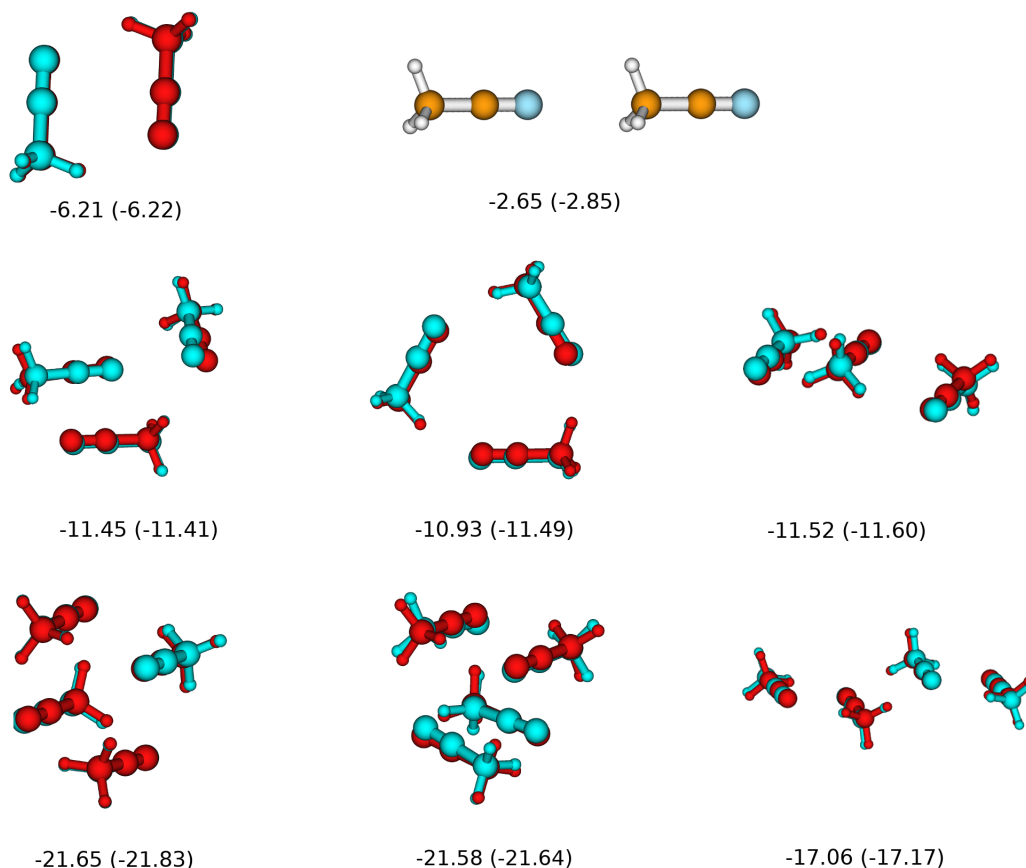


**Figure 4:** Comparison of the lowest energy structures of ACN clusters predicted by the force field (blue) and by the QM computations (red). The interaction energies in kcal/mol given by the ACN developed potential and the QM computations (value in parenthesis) are presented.

of the rest of geometrical parameters in both QM and classical cases. The agreement between both models is noticeable, in particular bearing in mind that they have been generated by the independent geometry optimization of each method, supporting the quality of the fit. Examining the curves it can be seen that at long distances, greater than 10 Å, there is not significant interaction energy. At an intermediate distance range, 5-9 Å, a distorted head to tail orientation favouring an incipient methyl hydrogen-nitrogen intermolecular bond is the most favored structure. At the distance range enclosing the minimum, 3-4 Å, an antiparallel orientation occurs, whereas at shorter distances an out of the plane orientation appears.

The second test on the developed potential concerns the preferred structures for small ACN clusters and their comparison with the corresponding QM results. This is presented in Figure 4, where the lowest energy  $(ACN)_n$  ( $n=2-4$ ) clusters are displayed. It is observed that QM (red) and force field (blue) predicted structures overimpose. The QM interaction energy is also very well reproduced by the classical force field. The largest difference corresponds to the head to tail trimer with a relative error is of  $\sim 5\%$ . It should be noted that the head to tail dimer is not a minimum for the force field, although its interaction energy is quite close to the QM one. In fact, we have examined the QM barrier for the conversion of the head to tail to the antiparallel structure, and it is only 0.1 kcal/mol. This highlights the difficulty for capturing this isomer. Even in this case the interaction energy is well reproduced and from a statistical point of view, this conformation does not appear to be significant.

Another illustrative test of the developed force field is the comparison of the predicted interaction energies with those of Remya and Suresh[39] on a wide set of ACN clusters. This set includes multiple aggregates, going from dimers

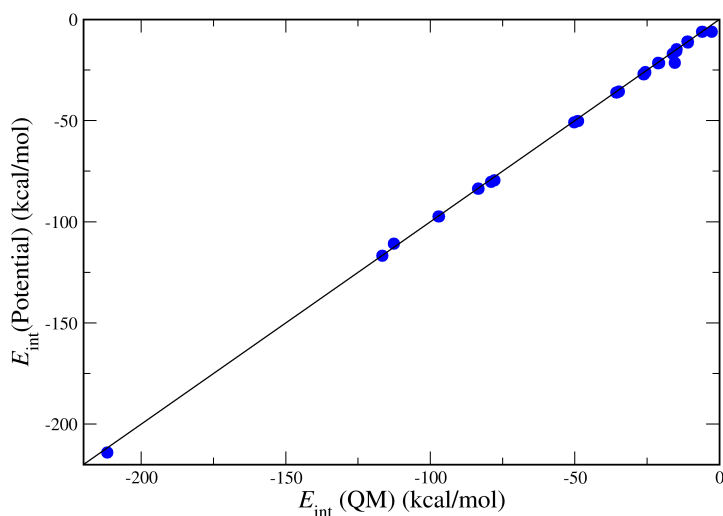


**Figure 5:** Comparison of the interaction energy (kcal/mol) of  $(\text{ACN})_n$  clusters ( $n=2-27$ ) predicted by the potential-derived in this work and those computed quantum-mechanically in ref.[39].

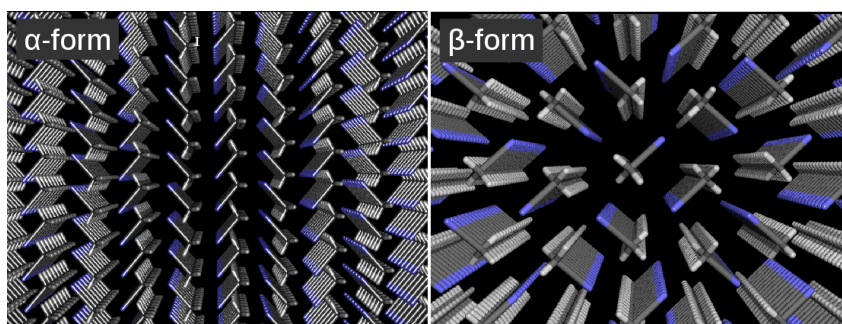


**Figure 6:** Crystal structures of ACN,  $\alpha$ -form (left) and  $\beta$ -form (right)

1 to hexadecamers and even 27-mer computed at the M06L/6-311++G(d,p) DFT level. Figure 5 shows the comparison  
 2 of the interaction energies given by our force field and those at the QM level given by Remya and Suresh[39]. Table  
 3 S2 in SM collects the numerical value for the different clusters using the original labelling given by the authors. The  
 4 agreement is quite satisfactory along the wide range of clusters examined dealing with a range of interaction energies  
 5 between -2.63 kcal/mol and -211.72 kcal/mol. This good agreement in a set of aggregates that were not included in the  
 6 fitting surface, but for the optimal dimers and trimer set, gives us strong confidence in the performance of the classical  
 7 potential for gas phase studies.

### 8 **3.2. Solid Phase**

9 227 K is the ACN melting point, below this temperature two crystalline forms have been characterized, the  $\alpha$ -  
 10 and the  $\beta$ -form with a phase transition occurring at 216.9 K. The  $\alpha$ -form is the structure stable at temperatures below the  
 11 phase transition temperature, whereas the  $\beta$ -form is present in the short range between the melting point and phase  
 12 transition temperatures.[28–30] Figure 6 displays the two structures, the  $\alpha$ -form has a monoclinic cell and a  $P2_1/c$   
 13 space group, whereas the  $\beta$ -form is orthorhombic in a  $Cmc2_1$  space group.[30] We generated, from the corresponding  
 14 unit cells, fragments of the  $\alpha$ - and  $\beta$ -forms including a total of 256 and 512 ACN molecules respectively. The first  
 15 test of our potential was the geometrical relaxation of both forms. Both kept their structural properties, and yield an

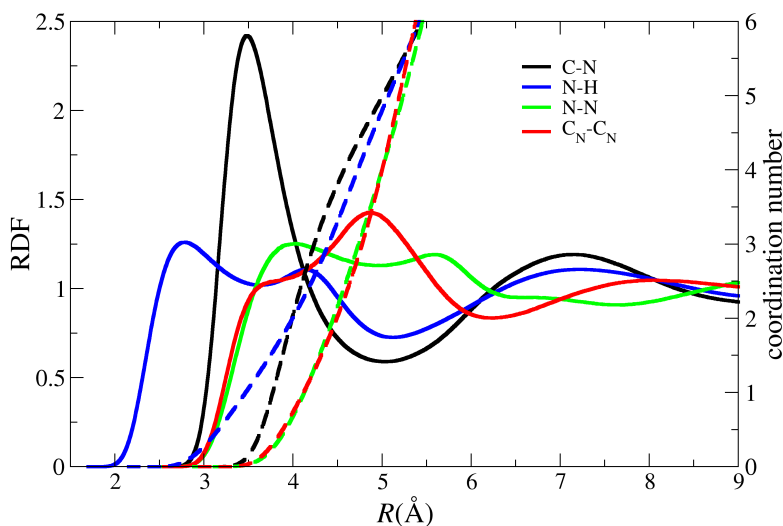
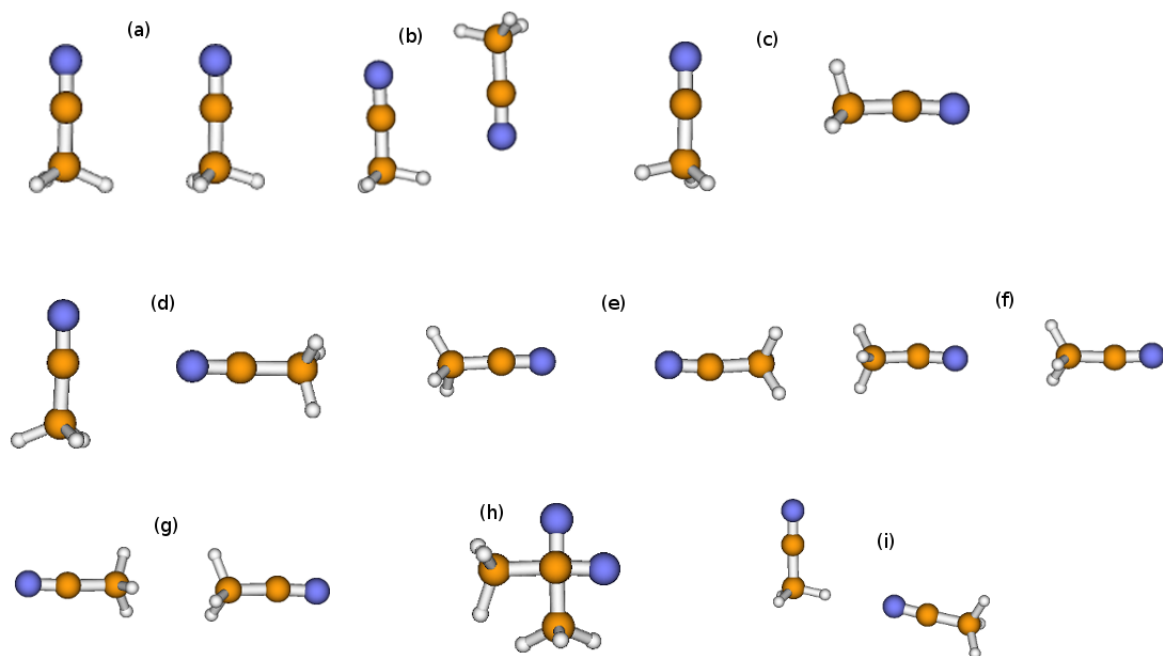


Figure 7: Main radial distribution functions of liquid ACN.

1 interaction energy per molecule of  $-11.42$  and  $-11.08$  kcal/mol for the  $\alpha$ - and  $\beta$ -form, respectively. This agrees with the  
 2 experimental evidence of the relative higher stability of the  $\alpha$ -form with respect to the  $\beta$ -form.[28–30] A second test  
 3 of the developed force field has been to carry out MD simulations of both solid ACN forms. From the previous relaxed  
 4 structures, 100 ps were run for equilibration at 200 K and 500 ps were run for analysis. Both forms kept their structures  
 5 and symmetry properties at 200 K, a temperature close to the melting point, giving confidence on the ability of the  
 6 classical model to reproduce the solid phase. Of course, at this temperature the  $\beta$ -form is expected to be unfavoured,  
 7 and the phase transition should occur. However such a process did not occur in the simulation time frame. In anycase,  
 8 what is important is the preservation of the solid structures. The average interaction energy per molecule derived  
 9 from MD simulations are  $-7.73$  and  $-7.60$  kcal/mol for the  $\alpha$ - and  $\beta$ -form, respectively. The relative energy difference,  
 10  $0.13$  kcal/mol, is very close to the experimental phase transition value of  $0.21$  kcal/mol.[50] The average structure of  
 11 the ACN molecule in the two forms is similar within the distribution uncertainty and agrees well with the experimental  
 12 values determined by Enjalbert and Galy in their X-ray study,[30]:  $R(\text{C-H}) = 1.09 \pm 0.02$  Å [ $1.02$  Å ( $\alpha$ ) and  $1.08$  Å  
 13 ( $\beta$ )];  $R(\text{C-C}) = 1.46 \pm 0.02$  Å [ $1.45$  Å ( $\alpha$ ) and  $1.44$  Å ( $\beta$ )];  $R(\text{C-N}) = 1.17 \pm 0.01$  Å [ $1.14$  Å ( $\alpha$ ) and  $1.15$  Å ( $\beta$ )].

### 14 3.3. Liquid Phase

15 Figure 7 shows the most illustrative interatomic pair correlation functions (left axis) together with their  
 16 coordination numbers (right axis). The most structured RDF is that involving the methyl carbon and nitrogen (black  
 17 line) presenting a well defined peak at  $\sim 3.4$  Å. This corresponds roughly to a head to tail arrangement, with a  
 18 predominant orientation towards one of methyl hydrogen as observed in the N-H RDF (blue line), that presents two  
 19 peaks, the first centered at  $\sim 2.7$  Å and the second at  $\sim 4.1$  Å. The corresponding coordination number roughly  
 20 integrates to the 3 hydrogen atoms of the methyl group after these two peaks. This suggests an arrangement where  
 21 one ACN molecule coordinates with its nitrogen atom to a hydrogen atom of another tilted ACN molecule, i.e. a  
 22 weak hydrogen bond interaction already pointed out by other authors.[14, 16, 26, 38, 39] The nitrile carbon ( $\text{C}_\text{N}$ ) is the  
 23 nucleus closer to the molecular center of mass, shifted only  $0.27$  Å. The  $\text{C}_\text{N}$ - $\text{C}_\text{N}$  RDF (red line) may then be considered  
 24 as representative of the mean separation among molecules in the liquid state, having a maximum at  $4.9$  Å, although a  
 25 shoulder at shortest distance,  $\sim 3.6$  Å that integrates to 0.5, collects the small fraction of antiparallel dimers present  
 26 in the liquid. RDFs provided by other authors[12, 14, 16, 18, 23, 24] in the literature are similar to those in Figure 7,  
 27 except for the  $\text{C}_\text{N}$ - $\text{C}_\text{N}$  one, or its equivalent center of mass-center of mass. For this RDF we obtain a wide peak with  
 28 a maximum at  $5.0$  Å and a previous hump at  $3.5$  Å, this morphology is absent in other works where a wide unsplit peak



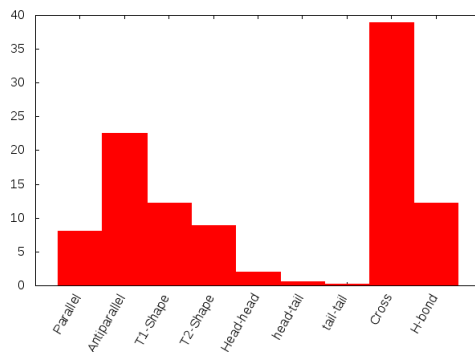
**Figure 8:** Types of dimer arrangements: (a) Parallel, (b) Antiparallel, (c) T1-shaped, (d) T2-shaped, (e) Head-head, (f) Head-tail, (g) Tail-tail, (h) Cross, (i) H-bond

is present,[13, 16, 18–20, 23, 24] on the contrary, Cabaleiro-Lago et al.[21], Koverga et al.[14], Pothoczki et al.[12] find a more convoluted peak but with similar morphology.

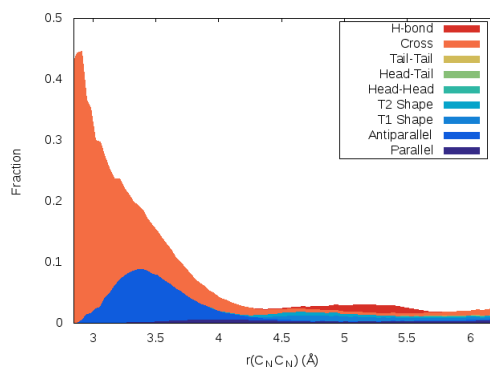
A second type of interesting structural information in the case of ACN, due to its cylindrical shape, is the analysis of the relative orientational correlation as a function of the intermolecular distance. The easiest way to quantify the different types of dimer arrangements is based on the angles formed between the two molecular axis (dipole vectors) and the angle connecting the line joining the center of mass of the two molecules and one of the molecular axis. For our analysis we have adopted the definition given by Pothoczki et al.[12, 51]. Figure 8 displays the different orientations. We have included another orientation corresponding to a weak hydrogen bond formed by C-H...N (arrangement (i)). The geometrical criterium to consider one structure of this type is  $R(H...N)$  in the interval 2.0-2.5 Å and the angle formed by the C-H and N-C<sub>N</sub> bonds in the interval -15 - +15°. Figure 9 shows a histogram of the average numbers of dimers of a given type found among the ACN molecules which are inside the first solvation shell, i.e. molecules whose C<sub>N</sub> are separated less than 6.25 Å (see C<sub>N</sub>-C<sub>N</sub> RDF in Figure 7) It is observed that the cross and antiparallel types are those with the highest occurrence, T1-shaped and H-bonds being the secondmore common types of arrangements. At first sight, this distribution could seem far apart from the results of other authors[12–14] but we must point out that we are dealing with the relative distribution inside the whole first solvation shell. The global picture rather suggests that there is no a real dominant orientation inside this first shell.

Figure 10 displays the normalized distribution of the different dimer arrangements as a function of the C<sub>N</sub>-C<sub>N</sub> distance, i.e. roughly the separation of the center of mass of the two molecules. It must be mentioned that the plotted functions for each dimer corresponds to the visible wide of its function, i.e., at 3.4 Å the distribution for the antiparallel arrangement is 0.1 and the value for the cross type is roughly 0.1. Curves are accumulative. In the interval 3.3-3.8 Å the antiparallel orientation is dominant, as reported by previous studies.[12–14] Going to longer distances the other dimer types appear with low frequency. The most noticeable result of this long-range region is the non-negligible contribution of the H-bond type, particularly in the 5.0-5.5 Å region. This supports the analysis performed by Kowsari et al.[13] on the evidence of a weak hydrogen bond (N...H-C) formation what was also suggested by Koverga et al.[14].

## Simulation of acetonitrile in liquid, gas and solid phases



**Figure 9:** Histogram of the different types of dimers present in the first solvation shell.



**Figure 10:** Normalized appearance frequency of the different arrangements as a function of the  $C_N-C_N$  distance.

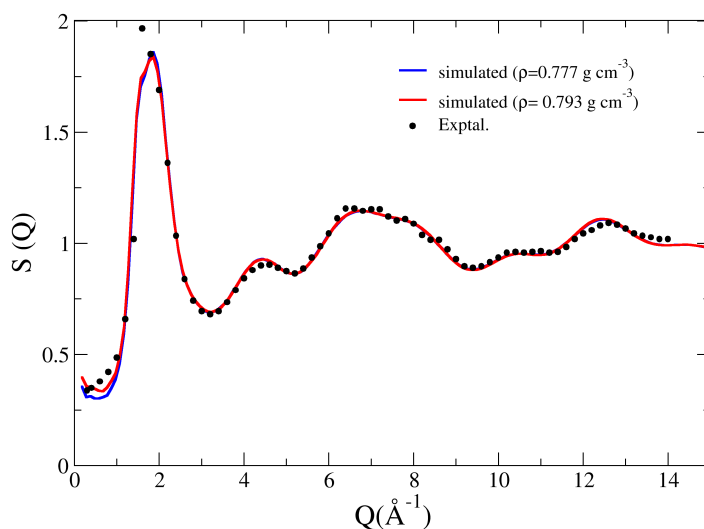
Table 3 collects a set of properties computed from the ACN liquid MD simulation at 298 K; energetics, structural and dynamical properties of the ensemble have been analyzed. For the sake of comparison, experimental values and theoretical results given by other authors have been included in the Table. It is worth pointing out the good behavior of the developed potential when dealing with a wide range of physicochemical properties in liquid state. Thus, a magnitude reflecting the energetics of the system as the vaporization enthalpy is predicted within the experimental range, as it is also found for a mechanical property such as the isothermal compressibility which was computed as described by Guàrdia et al.[19] Dynamical properties such as the translational diffusion coefficient, reorientational times corresponding to the dipole moment axis or viscosity are quite close to the observed experimental range. It must be stressed that box-size correction of diffusion coefficient has employed the computed value of viscosity. Thus, the good behavior of  $D$  represents a double-check on the consistency of the estimated values derived from our simulation. Only three previous simulations have estimated the average dipole moment in the liquid.[20, 21, 58] Our estimation being the most accurate value from a simulation up to the present.

An additional test is the computation of neutron diffraction data of ACN liquid for its isotopic substitution  $CD_3C^{14}N$ . A set of 1000 evenly-spaced snapshots of our MD simulation were introduced as structural information in the ISAACS code[63] for computing the neutron diffraction data. It has been checked that the use of a larger number of snapshots does not change the results. Figure 11 plots the experimental data recorded by Bertagnolli et al.[8] at 293 K, and later used by Pothoczki and Pusztai[12] in their combined study of all-atom simulations and diffraction measurements. Two simulations of the neutron diffraction data of liquid ACN have been performed considering either the structures of the NPT MD simulation, that corresponds to a density value of  $0.793 \text{ g/cm}^3$  and that of the NVT MD simulation whose density is the experimental value at 298 K,  $0.777 \text{ g/cm}^3$ . The agreement among the different curves is really good and allows us to conclude that the 5 K difference between experimental and simulated neutron data is not significant, neither

**Table 3**

Basic properties of liquid ACN at 298 K.

Property <sup>o</sup>	MD simulation	Literature	Exptal.
$\Delta H_{\text{vap}}$ (kJ mol <sup>-1</sup> )	-33.0	(-30.7)-(-34.2) <sup>a</sup>	(-32.9)-(-34.5) <sup>b</sup>
$\rho$ (kg m <sup>-3</sup> )	793	718-776 <sup>c</sup>	776-778 <sup>d</sup>
$\kappa$ (GPa <sup>-1</sup> )	1.07	1.18-1.62 <sup>e</sup>	1.07-1.13 <sup>f</sup>
$\mu$ (D)	4.67	4.01-4.88 <sup>g</sup>	4.5 <sup>h</sup>
$D \cdot 10^9$ (m <sup>2</sup> s <sup>-1</sup> )	3.81	3.02-4.93 <sup>i</sup>	4.04-5.10 <sup>j</sup>
$\tau_1$ (ps)	3.9		3.28-3.68 <sup>k</sup>
$\tau_2$ (ps)	1.3		1.02 <sup>l</sup>
$\eta$ (cP)	0.43	0.29-0.64 <sup>m</sup>	0.34 <sup>n</sup>

<sup>a</sup>Refs.[14, 15, 17, 20, 52, 53] <sup>b</sup>Refs.[54, 55] <sup>c</sup>Refs.[14, 15, 17, 20, 27, 52, 53]<sup>d</sup>Refs.[13, 55, 56] <sup>e</sup>Refs.[52] <sup>f</sup>Refs.[57] <sup>g</sup>Refs.[20, 21, 58] <sup>h</sup>Refs.[59]<sup>i</sup>Refs.[14, 15, 17, 20, 52, 53] <sup>j</sup> compilation in Ref.[13] <sup>k</sup>Refs.[60, 61] <sup>m</sup>Ref.[18, 19, 23, 24]<sup>n</sup>Ref.[62]<sup>o</sup>vaporization enthalpy,  $\Delta H_{\text{vap}}$ ; density,  $\rho$ ; isothermal compressibility,  $\kappa$ ;  
dipole moment,  $\mu$ ; diffusion coefficient,  $D$ ;1st. and 2nd. dipole moment axis reorientational times,  $\tau_1$  and  $\tau_2$ ;  $\eta$ , viscosity.**Figure 11:** Neutron diffraction data for liquid ACN at 293K: experiment (black dots) taken from ref. [8], simulated data from NPT MD simulation (red line) and from NVT MD simulation with the experimental density (blue line)

1 the slight density change between the NPT and NVT simulated functions. It is worthy to comment that Pothoczki and  
 2 Pusztai[12] using the six-site OPLS force field of Jorgensen and col.[64] computed the X-ray and neutron diffraction  
 3 data of ACN obtaining an excellent agreement with the experimental data.

4 Since the developed force field uses a flexible and polarizable molecular model for ACN, a final analysis has been  
 5 the inspection of how the average dipole moment of ACN molecules,  $\langle \mu \rangle$ , changes for the different phases. This  
 6 evolution is presented in Figure 12 where the mean dipole moment for the set of gas phase clusters previously examined  
 7 in Figure 5 is plotted as a function of the number of molecules forming the aggregate. The vertical bars correspond to  
 8 the dispersion of the individual dipole moments present in the clusters considered. It should be noted that the  $\langle \mu \rangle$   
 9 increases with the cluster converging to a value close to that of the liquid MD simulation. This is not the case for the  
 10 27-mer cluster that presents an average dipole moment value larger than the mean liquid value. This is due to the fact



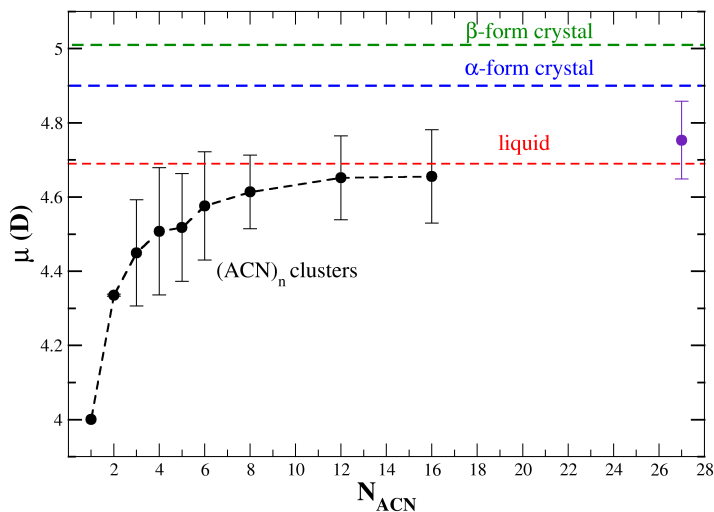


**Figure 12:** Evolution of the average dipole moment (D) of ACN molecule with the cluster size, indigo dot corresponds to a  $(ACN)_{27}$  cluster with the structure corresponding to the ACN crystal arrangement. Vertical bars indicates the range of dipole values of molecules in a given cluster. Horizontal dashed lines indicates the mean value of dipole moment in liquid at 300K (red) and in the  $\alpha$  (blue) and  $\beta$  crystals (green).

1 that the structure of this cluster is a fragment of the  $\alpha$ -form crystal structure, where dipole alignment is predominant  
 2 (see Figure 6). This fact is confirmed by the computed mean value of the crystal  $\alpha$ -form (blue line) which is larger than  
 3 that of the liquid and the 27-mer cluster. Finally the structural arrangement of the  $\beta$ -form leads to a higher average  
 4 dipole moment. Apart from an intrinsic good description of the charge distribution provided by the force field for the  
 5 isolated molecule yielding 4.0 D vs. an experimental value of 3.96 D,[42] the molecular polarization of our model is  
 6 able to reproduce environmental effects progressively more complex by including many-body and temperature effects.

#### 7 4. Concluding remarks

8 This study has shown the validity of a new flexible and polarizable force field to deal with the three states of  
 9 matter of acetonitrile based on first principles calculations exclusively. It has been shown that the MCDHO strategy  
 10 is versatile enough to grasp the polarizable character of acetonitrile under different environments, going from small  
 11 molecular aggregates to either liquid at room temperature or two crystalline forms. Hence this study highlights the  
 12 importance of a good description of both, the electronic polarization and the intramolecular flexibility together with  
 13 the explicit inclusion of many-body contributions. This permits the proper reproduction of the molecular and bulk  
 14 behavior at different phases. It is also shown that a proper molecular description of the acetonitrile can be reached  
 15 without including experimental information in the force field building, although a sophisticated formalism was needed  
 16 to develop it.

17 The consistency of the potential supports two conclusions. Contrary to the case of the ubiquitous solvent, water,  
 18 quantum-mechanical ingredients incorporated through the MP2 method with a large even-tempered basis sets is enough  
 19 to describe both the molecular and the condensed phase behavior of acetonitrile. The second conclusion is that many-  
 20 body effects can be incorporated by explicit molecular polarizability and a limited number of acetonitrile molecules  
 21 in the clusters considered in the ab initio potential surfaces used for the fitting.

22 The structural analysis of liquid ACN reveals that its structure extends to the first solvation shell where a dominant  
 23 pair-orientation does not exist, antiparallel, cross, H-bond and T1-shaped being the more frequent arrangements as a  
 24 function of the intermolecular distance.

The classical nature of the potential will allow the exploration of highly-demanding computational properties of acetonitrile liquid, as dielectric and rheological properties, because of the large number of molecules to be considered or the need of long simulation times are affordable. The high-level *ab initio* nature of the information employed to characterize the ACN molecule and its interactions with other molecules under many different arrangements allows a refined and unbiased molecular answer in different environments.

The combination of the two previous feature potential leads to the conclusion that this potential gives an even-tempered description of ACN-containing systems where a compromise between condensed phase factors and molecular properties simultaneously contribute to the physicochemical properties of the system. Then future efforts will be addressed to find out the limits of the force field by computing significant bulk-depending mechanical, dynamical, electric, magnetic, rheological and spectroscopic properties of acetonitrile under a wide range of temperature and pressure. In addition, this potential could be applied in multicomponent systems in different aggregation states: gas, solutions, confined media, interphases and solid and crystalline systems.

## 5. Acknowledgements

We thank Dr. Silvia Pothoczki for providing us the experimental neutron diffraction data of liquid acetonitrile. We are grateful to Reyes Garcia Carreon for support in the computational part of this work. This document is the result of the research project (PGC2018-099366-B-I00) funded by the Spanish Ministry of Science, Innovation and Universities and by the Universidad Nacional Autónoma de México (UNAM) (DGAPA-PAPIIT-IG100920) and Project LANCAD-UNAM-DGTIC-057 for computational resources.

## 6. Appendix A. Supplementary data

Supplementary data to this article can be found online at

## References

- [1] C. Reichardt, *Solvent and Solvent Effects in Organic Chemistry*, 2nd ed., Wiley-VCH, Weinheim, 2004.
- [2] N. Kumar, D. Sangeetha, P. Balakrishna, Development and validation of a UPLC method for the determination of duloxetine hydrochloride residues on pharmaceutical manufacturing equipment surfaces, *Pharm. Methods* 2 (2010) 161–166.
- [3] L. Wannatong, A. Sirivat, P. Supaphol, Effects of solvents on electrospun polymeric fibers: preliminary study on polystyrene, *Pharm. Methods* 53 (2004) 1851–1859.
- [4] J. Kim, D.-J. Lee, H.-G. Jung, Y.-K. Sun, J. Hassoun, B. Scrosati, Lithium-sulfur batteries: an advanced lithium-sulfur battery, *Adv. Funct. Mater.* 23 (2013) 1076–1080.
- [5] G. Caldwell, M. D. Rozeboom, J. P. Kiplinger, J. E. Bartmess, Displacement, proton transfer, or hydrolysis? mechanistic control of acetonitrile reactivity by stepwise solvation of reactants, *J. Am. Chem. Soc.* 106 (1984) 809–810.
- [6] R. Bogseth, E. Edgcomb, C. M. Jones, E. K. Chess, P. Hu, Acetonitrile adduct formation as a sensitive means for simple alcohol detection by LC-MS, *J. Am. Soc. Mass Spectrom.* 25 (2014) 1987–1990.
- [7] S. Pothoczki, L. Temleitner, L. Pusztai, Structure of neat liquids consisting of (perfectly and nearly) tetrahedral molecules, *Chem. Rev.* 115 (2015) 13308–13361.
- [8] H. Bertagnolli, P. Chieux, M. D. Zeidler, Neutron-diffraction study of liquid acetonitrile I.  $\text{CD}_3\text{C}^{14}\text{N}$ , *Mol. Phys.* 32 (1976) 759–773.
- [9] H. Bertagnolli, P. Chieux, M. D. Zeidler, Neutron-diffraction study of liquid acetonitrile II.  $\text{CD}_3\text{C}^{15}\text{N}$ , *Mol. Phys.* 32 (1976) 1731–1736.
- [10] H. Bertagnolli, M. D. Zeidler, Molecular pair-correlation function of liquid acetonitrile from x-ray and neutron-diffraction studies., *Mol. Phys.* 35 (1978) 177–192.
- [11] T. Radnai, S. Itoh, H. Ohtaki, Liquid structure of N,N-dimethylformamide, acetonitrile and their 1:1 molar mixture., *Bull. Chem. Soc. Jpn.* 61 (1988) 3845–3852.
- [12] S. Pothoczki, L. Pusztai, Intermolecular orientations in liquid acetonitrile: New insights based on diffraction measurements and all-atom simulations, *J. Mol. Liq.* 225 (2017) 160–166.
- [13] M. Kowsari, L. Tohidifar, Systematic evaluation and refinement of existing all-atom force fields for the simulation of liquid acetonitrile, *J. Comput. Chem.* 39 (2018) 1843–1853.
- [14] V. A. Koverga, O. M. Korsun, O. Kalugin, B. Marekha, A. Idrissi, A new potential model for acetonitrile: Insight into the local structure organization, *J. Mol. Liq.* 233 (2017) 251–261.
- [15] M. Orhan, Dielectric and transport properties of acetonitrile at varying temperatures: a molecular dynamics study, *Bull. Korean Chem. Soc.* 35 (2014) 1469–1478.
- [16] M. Albertí, A. Amat, F. De Angelis, F. Pirani, A model potential for acetonitrile: from small clusters to liquid, *J. Phys. Chem. B* 117 (2013) 7065–7076.
- [17] A. M. Nikitin, A. Lyubartsev, New six-site acetonitrile model for simulations of liquid acetonitrile and its aqueous mixtures, *J. Comput. Chem.* 28 (2007) 2020–2026.
- [18] P. J. Gee, W. van Gusteren, Acetonitrile revisited: a molecular dynamics study of the liquid phase, *Mol. Phys.* 104 (2006) 477–483.

- [19] E. Guàrdia, R. Pinzón, J. Casulleras, M. Orozco, F. Luque, Comparison of different three-site interaction potentials for liquid acetonitrile, *Mol. Simul.* 26 (2001) 287–306.
- [20] X. Grabuleda, C. Jaime, P. A. Kollman, Molecular dynamics simulation studies of liquid acetonitrile: New six-site model, *J. Comput. Chem.* 21 (2000) 901–908.
- [21] E. Cabaleiro-Lago, M. Ríos, Intermolecular potential for acetonitrile based on ab initio calculations, *Mol. Phys.* 96 (1999) 309–321.
- [22] J. Siebers, U. Buck, T. Beu, Calculation of structures and vibrational spectra of acetonitrile clusters, *Chem. Phys.* 239 (1998) 549–560.
- [23] W. L. Jorgensen, J. M. Briggs, Monte carlo simulations of liquid acetonitrile with a three-site model, *Mol. Phys.* 63 (1988) 547–558.
- [24] D. Edwards, P. A. Madden, I. McDonald, A computer simulation study of the dielectric properties of a model of methyl cyanide, *Mol. Phys.* 51 (1984) 1141–1161.
- [25] H. Böhm, I. McDonald, P. A. Madden, An effective pair potential for liquid acetonitrile, *Mol. Phys.* 49 (1983) 347–360.
- [26] J. Chen, P. Sit, Ab initio study of the structural properties of acetonitrile-water mixtures, *Chem. Phys.* 457 (2015) 87–97.
- [27] R. Dias, C. da Costa, T. Manhabosco, A. de Oliveira, M. Matos, J. Soares, R. J. Batista, Ab initio molecular dynamics simulation of methanol and acetonitrile: the effect of van der Waals interactions, *Chem. Phys. Lett.* 714 (2019) 172–177.
- [28] M. Barrow,  $\alpha$  acetonitrile at 215 K, *Acta Cryst. B37* (1981) 2239–2242.
- [29] O. K. Antson, K. J. Till, N. H. Andersen, Neutron powder diffraction study of deuterated  $\beta$ -acetonitrile, *Acta Cryst. B43* (1987) 296–301.
- [30] R. Enjalbert, J. Galy, CH<sub>3</sub>CN: X-ray structural investigation of a unique single crystal.  $\beta \rightarrow \alpha$  phase transition and crystal structure, *Acta Cryst. B58* (2002) 1005–1010.
- [31] M. Hloucha, A. K. Sum, S. I. Sandler, Computer simulation of acetonitrile and methanol with ab initio-based pair potentials, *J. Chem. Phys.* 113 (2000) 5401–5406.
- [32] H. Saint-Martin, J. Hernández-Cobos, M. I. Bernal-Uruchurtu, I. Ortega-Blake, H. J. C. Berendsen, A mobile charge densities in harmonic oscillators (MCDHO) molecular model for numerical simulations: The water–water interaction, *J. Chem. Phys.* 113 (2000) 10899–10912.
- [33] H. Saint-Martin, J. Hernández-Cobos, I. Ortega-Blake, Water models based on a single potential energy surface and different molecular degrees of freedom, *J. Chem. Phys.* 122 (2005) 224509(1)–224509(12).
- [34] M. Valdéz-González, H. Saint-Martin, J. Hernández-Cobos, R. Ayala, E. Sánchez Marcos, I. Ortega-Blake, Liquid methanol Monte Carlo simulations with a refined potential which includes polarizability, nonadditivity, and intramolecular relaxation, *J. Chem. Phys.* 127 (2007) 224507(1)–224507(14).
- [35] E. Galbis, J. Hernández-Cobos, R. Pappalardo, E. Sanchez Marcos, Collecting high-order interactions in an effective pairwise intermolecular potential using the hydrated ion concept: The hydration of Cf(III), *J. Chem. Phys.* 140 (2014) 214104–(1)–(11).
- [36] M. J. Frisch, G. W. Trucks, H. B. Schlegel, G. E. Scuseria, M. A. Robb, J. R. Cheeseman, G. Scalmani, V. Barone, B. Mennucci, G. A. Petersson, H. Nakatsuji, M. Caricato, X. Li, H. P. Hratchian, A. F. Izmaylov, J. Bloino, G. Zheng, J. L. Sonnenberg, M. Hada, M. Ehara, K. Toyota, R. Fukuda, J. Hasegawa, M. Ishida, T. Nakajima, Y. Honda, O. Kitao, H. Nakai, T. Vreven, J. A. Montgomery, Jr., J. E. Peralta, F. Ogliaro, M. Bearpark, J. J. Heyd, E. Brothers, K. N. Kudin, V. N. Staroverov, R. Kobayashi, J. Normand, K. Raghavachari, A. Rendell, J. C. Burant, S. S. Iyengar, J. Tomasi, M. Cossi, N. Rega, J. M. Millam, M. Klene, J. E. Knox, J. B. Cross, V. Bakken, C. Adamo, J. Jaramillo, R. Gomperts, R. E. Stratmann, O. Yazyev, A. J. Austin, R. Cammi, C. Pomelli, J. W. Ochterski, R. L. Martin, K. Morokuma, V. G. Zakrzewski, G. A. Voth, P. Salvador, J. J. Dannenberg, S. Dapprich, A. D. Daniels, Farkas, J. B. Foresman, J. V. Ortiz, J. Cioslowski, D. J. Fox, Gaussian 09 Revision D.01, 2009. Gaussian Inc. Wallingford CT.
- [37] E. Cabaleiro-Lago, J. Hermida-Ramón, A. Peña Gallego, E. Martínez-Nuñez, A. Fernández-Ramos, Intermolecular interactions and cooperative effects in acetonitrile clusters. an based ab initio molecular orbital study, *J. Mol. Struct. (Theochem)* 498 (2000) 21–28.
- [38] R. A. Mata, B. Costa Cabral, Structural, energetic, and electronic properties of (CH<sub>3</sub>CN)<sub>2-8</sub> clusters by density functional theory, *J. Mol. Struct. (Theochem)* 673 (2004) 155–164.
- [39] K. Remya, C. H. Suresh, Cooperativity and cluster growth patterns in acetonitrile: A dft study., *J. Comput. Chem.* 35 (2014) 910–922.
- [40] S. N. Ghosh, R. Trambarulo, W. Gordy, Electric dipole moments of several molecules from the stark effect, *J. Chem. Phys.* 21 (1953) 308–310.
- [41] C. C. Costain, Determination of molecular structures from ground state rotational constants, *J. Chem. Phys.* 29 (1958) 864–874.
- [42] A. D. Buckingham, R. E. Raab, The dielectric polarization of some imperfect polar gases, *J. Chem. Soc.* (1961) 5511–5523.
- [43] T. B. Freedman, E. R. Nixon, Matrix isolation studies of methyl cyanide in solid argon and methyl isocyanide, *Spectrochim. Acta* 28A (1973) 1375–1391.
- [44] T. A. Renner, M. Blander, A study of dimerization in acetonitrile vapor by measurement of thermal conductivity, *J. Phys. Chem.* 81 (1977) 857–861.
- [45] I. T. Todorov, W. Smith, K. Trachenko, M. T. Dove, DL\_POLY\_3: New dimensions in molecular dynamics simulations via massive parallelism, *J. Mat. Chem.* 16 (2006) 1911–1918.
- [46] D. Frenkel, B. Smit, Understanding Molecular Simulation. from Algorithms to Applications, 2nd ed., Academic Press, San Diego, USA, 2002.
- [47] I.-C. Yeh, and Gerhard Hummer, System-Size Dependence of Diffusion Coefficients and Viscosities from Molecular Dynamics Simulations with Periodic Boundary Conditions, *J. Phys. Chem. B* 108 (2004) 15873–15879.
- [48] M. P. Allen, D. J. Tildesley, Computer Simulation of Liquids, Oxford University Press, Oxford, 1987.
- [49] Y. Zhang, A. Otani, E. J. Maginn, Reliable viscosity calculation from equilibrium molecular dynamics simulations: A time decomposition method, *J. Chem. Theory Comput.* 11 (2015) 3537–3546.
- [50] W. E. Putnam, D. M. McEachern, J. E. Kilpatrick, Entropy and related thermodynamic properties of acetonitrile (methyl cyanide), *J. Chem. Phys.* 42 (1965) 749–755.
- [51] S. Pothoczki, L. Temleitner, L. Pusztai, Detailed intermolecular structure of molecular liquids containing slightly distorted tetrahedral molecules with  $c_{3v}$  symmetry: Chloroform, bromoform and methyl-iodide, *J. Chem. Phys.* 134 (2011) 044521.
- [52] C. Caleman, P. J. van Maaren, M. Hong, J. S. Hub, L. Costa, D. D. van der Spoel, Force field benchmark of organic liquids: density, enthalpy of vaporization, heat capacities, surface tension, isothermal compressibility, volumetric expansion coefficient, and dielectric constant, *J. Chem. Theory Comput.* 8 (2012) 61–74.

- 1 [53] M. Kowsari, L. Tohidifar, Tracing dynamics, self-diffusion, and nanoscale structural heterogeneity of pure and binary mixtures of ionic liquid  
2 1-hexyl-2,3-dimethylimidazolium bis(fluorosulfonyl)imide with acetonitrile: Insights from molecular dynamics simulations, *J. Phys. Chem.*  
3 *B* 120 (2016) 10824–10838.
- 4 [54] X.-W. An, M. Månsson, Enthalpies of combustion and formation of acetonitrile, *J. Chem. Thermodyn.* 15 (1983) 287–293.
- 5 [55] DDBST GmbH webpage, Dortmund data bank, 2019. [Http://www.ddbst.com/en/EED/PCP/DEN-C3.php](http://www.ddbst.com/en/EED/PCP/DEN-C3.php).
- 6 [56] R. W. Gallant, Physical properties of hydrocarbons .36. nitriles, *Hydrocarbons Processing* 48 (1969) 135.
- 7 [57] Y. Marcus, *The Properties of Solvents*, Wiley, New York, 1998.
- 8 [58] R. Rivelino, B. Costa Cabral, K. Coutinho, S. Canuto, Electronic polarization in liquid acetonitrile: A sequential Monte Carlo/quantum  
9 mechanics investigation, *Chem. Phys. Lett.* 407 (2005) 13–17.
- 10 [59] Y. Fujita, T. Ohba, S. Ikawa, Measurements of far-infrared optical constants of liquids with a synchrotron radiation source, *Can. J. Chem.* 69  
11 (1991) 1745–1751.
- 12 [60] P. Yuan, M. Schwartz, Molecular reorientation in acetonitrile. a comparison of diffusion coefficients from raman bandshapes and nuclear  
13 magnetic resonance relaxation times, *J. Chem. Soc. Farady Trans.* 86 (1990) 593–596.
- 14 [61] A. Sugitani, S. Ikawa, S. Konaka, Effect of temperature on the infrared band shapes and reorientational and vibrational relaxation of liquid  
15 acetonitrile, *Chem. Phys.* 142 (1990) 423–430.
- 16 [62] H. Shekaari, M. T. Zafarani-Moattar, S. Mirheydari, Density, viscosity, speed of sound, and refractive index of a ternary solution of aspirin,  
17 1-butyl-3-methylimidazolium bromide, and acetonitrile at different temperatures  $t = (288.15 \text{ to } 318.15) \text{ K}$ , *J. Chem. Eng. Data* 60 (2015)  
18 1572–1583.
- 19 [63] S. Le Roux, V. Petkov, ISAACS – interactive structure analysis of amorphous and crystalline systems, *J. Appl. Cryst.* 43 (2010) 181–185.
- 20 [64] W. L. Jorgensen, D. S. Maxwell, J. Tirado-Rives, Development and testing of the opls all-atom force field on conformational energetics and  
21 properties of organic liquids, *J. Am. Chem. Soc.* 118 (1996) 11225–11236.